The Astrophysical Journal, 711:64–74, 2010 March 1 doi:10.1088/0004-637X/711/1/64

PSR J1907+0602: A RADIO-FAINT GAMMA-RAY PULSAR POWERING A BRIGHT TeV PULSAR WIND NEBULA

A. A. Abdo[1,2,63], M. Ackermann[3], M. Ajello[3], L. Baldini[4], J. Ballet[5], G. Barbiellini[6,7], D. Bastieri[8,9], B. M. Baughman[10], K. Bechtol[3], R. Bellazzini[4], B. Berenji[3], R. D. Blandford[3], E. D. Bloom[3], E. Bonamente[11,12], A. W. Borgland[3], J. Bregeon[4], A. Brez[4], M. Brigida[13,14], P. Bruel[15], T. H. Burnett[16], S. Buson[9], G. A. Caliandro[13,14], R. A. Cameron[3], F. Camilo[17], P. A. Caraveo[18], J. M. Casandjian[5], C. Cecchi[11,12], Ö. Çelik[19,20,21], A. Chekhtman[1,22], C. C. Cheung[19], J. Chiang[3], S. Ciprini[11,12], R. Claus[3], I. Cognard[23,24], J. Cohen-Tanugi[25], L. R. Cominsky[26], J. Conrad[27,28,64], S. Cutini[29], A. de Angelis[30], F. de Palma[13,14], S. W. Digel[3], B. L. Dingus[31], M. Dormody[32], E. do Couto e Silva[3], P. S. Drell[3], R. Dubois[3], D. Dumora[33,34], C. Farnier[25], C. Favuzzi[13,14], S. J. Fegan[15], W. B. Focke[3], P. Fortin[15], M. Frailis[30], P. C. C. Freire[35,36], Y. Fukazawa[37], S. Funk[3], P. Fusco[13,14], F. Gargano[14], D. Gasparrini[29], N. Gehrels[19,38], S. Germani[11,12], G. Giavitto[39], B. Giebels[15], N. Giglietto[13,14], F. Giordano[13,14], T. Glanzman[3], G. Godfrey[3], I. A. Grenier[5], M.-H. Grondin[33,34], J. E. Grove[1], L. Guillemot[33,34], S. Guiriec[40], Y. Hanabata[37], A. K. Harding[19], E. Hays[19], R. E. Hughes[10], M. S. Jackson[27,28,41], G. Jóhannesson[3], A. S. Johnson[3], T. J. Johnson[19,38], W. N. Johnson[1], S. Johnston[42], T. Kamae[3], H. Katagiri[37], J. Kataoka[43,44], N. Kawai[43,45], M. Kerr[16], J. Knödlseder[46], M. L. Kocian[3], M. Kuss[4], J. Lande[3], L. Latronico[4], M. Lemoine-Goumard[33,34], F. Longo[6,7], F. Loparco[13,14], B. Lott[33,34], M. N. Lovellette[1], P. Lubrano[11,12], A. Makeev[1,22], M. Marelli[18], M. N. Mazziotta[14], J. E. McEnery[19], C. Meurer[27,28], P. F. Michelson[3], W. Mitthumsiri[3], T. Mizuno[37], A. A. Moiseev[20,38], C. Monte[13,14], M. E. Monzani[3], A. Morselli[47], I. V. Moskalenko[3], S. Murgia[3], P. L. Nolan[3], J. P. Norris[48], E. Nuss[25], T. Ohsugi[37], N. Omodei[4], E. Orlando[49], J. F. Ormes[48], D. Paneque[3], D. Parent[33,34], V. Pelassa[25], M. Pepe[11,12], M. Pesce-Rollins[4], F. Piron[25], T. A. Porter[32], S. Rainò[13,14], R. Rando[8,9], P. S. Ray[1], M. Razzano[4], A. Reimer[50,3], O. Reimer[50,3], T. Reposeur[33,34], S. Ritz[32], M. S. E. Roberts[1,22,51], L. S. Rochester[3], A. Y. Rodriguez[52], R. W. Ro‘mani[3], M. Roth[16], F. Ryde[41,28], H. F.-W. Sadrozinski[32], D. Sanchez[15], A. Sander[10], P. M. Saz Parkinson[32], J. D. Scargle[53], C. Sgrò[4], E. J. Siskind[54], D. A. Smith[33,34], P. D. Smith[10], G. Spandre[4], P. Spinelli[13,14], M. S. Strickman[1], D. J. Suson[55], H. Tajima[3], H. Takahashi[37], T. Tanaka[3], J. B. Thayer[3], J. G. Thayer[3], G. Theureau[23], D. J. Thompson[19], L. Tibaldo[8,5,9], O. Tibolla[56], D. F. Torres[57,52], G. Tosti[11,12], A. Tramacere[3,58], Y. Uchiyama[59,3], T. L. Usher[3], A. Van Etten[3], V. Vasileiou[19,20,21], C. Venter[19,60], N. Vilchez[46], V. Vitale[47,61], A. P. Waite[3], P. Wang[3], K. Watters[3], B. L. Winer[10], M. T. Wolff[1], K. S. Wood[1], T. Ylinen[41,62,28], and M. Ziegler[32]

[1] Space Science Division, Naval Research Laboratory, Washington, DC 20375, USA; aous.abdo@nrl.navy.mil, malloryr@gmail.com, Kent.Wood@nrl.navy.mil
[2] National Research Council, National Academy of Sciences, Washington, DC 20001, USA
[3] W. W. Hansen Experimental Physics Laboratory, Kavli Institute for Particle Astrophysics and Cosmology, Department of Physics and SLAC National Accelerator Laboratory, Stanford University, Stanford, CA 94305, USA
[4] Istituto Nazionale di Fisica Nucleare, Sezione di Pisa, I-56127 Pisa, Italy
[5] Laboratoire AIM, CEA-IRFU/CNRS/Université Paris Diderot, Service d'Astrophysique, CEA Saclay, 91191 Gif sur Yvette, France
[6] Istituto Nazionale di Fisica Nucleare, Sezione di Trieste, I-34127 Trieste, Italy
[7] Dipartimento di Fisica, Università di Trieste, I-34127 Trieste, Italy
[8] Istituto Nazionale di Fisica Nucleare, Sezione di Padova, I-35131 Padova, Italy
[9] Dipartimento di Fisica "G. Galilei," Università di Padova, I-35131 Padova, Italy
[10] Department of Physics, Center for Cosmology and Astro-Particle Physics, The Ohio State University, Columbus, OH 43210, USA
[11] Istituto Nazionale di Fisica Nucleare, Sezione di Perugia, I-06123 Perugia, Italy
[12] Dipartimento di Fisica, Università degli Studi di Perugia, I-06123 Perugia, Italy
[13] Dipartimento di Fisica "M. Merlin" dell'Università e del Politecnico di Bari, I-70126 Bari, Italy
[14] Istituto Nazionale di Fisica Nucleare, Sezione di Bari, 70126 Bari, Italy
[15] Laboratoire Leprince-Ringuet, École polytechnique, CNRS/IN2P3, Palaiseau, France
[16] Department of Physics, University of Washington, Seattle, WA 98195-1560, USA
[17] Columbia Astrophysics Laboratory, Columbia University, New York, NY 10027, USA
[18] INAF—Istituto di Astrofisica Spaziale e Fisica Cosmica, I-20133 Milano, Italy
[19] NASA Goddard Space Flight Center, Greenbelt, MD 20771, USA
[20] Center for Research and Exploration in Space Science and Technology (CRESST), NASA Goddard Space Flight Center, Greenbelt, MD 20771, USA
[21] Department of Physics and Center for Space Sciences and Technology, University of Maryland Baltimore County, Baltimore, MD 21250, USA
[22] Center of Earth Observing and Space Research, College of Science, George Mason University, Fairfax, VA 22030, USA
[23] Laboratoire de Physique et Chemie de l'Environnement, LPCE UMR 6115 CNRS, F-45071 Orléans Cedex 02, France
[24] Station de radioastronomie de Nançay, Observatoire de Paris, CNRS/INSU, F-18330 Nançay, France
[25] Laboratoire de Physique Théorique et Astroparticules, Université Montpellier 2, CNRS/IN2P3, Montpellier, France
[26] Department of Physics and Astronomy, Sonoma State University, Rohnert Park, CA 94928-3609, USA
[27] Department of Physics, Stockholm University, AlbaNova, SE-106 91 Stockholm, Sweden
[28] The Oskar Klein Centre for Cosmoparticle Physics, AlbaNova, SE-106 91 Stockholm, Sweden
[29] Agenzia Spaziale Italiana (ASI) Science Data Center, I-00044 Frascati (Roma), Italy
[30] Dipartimento di Fisica, Università di Udine and Istituto Nazionale di Fisica Nucleare, Sezione di Trieste, Gruppo Collegato di Udine, I-33100 Udine, Italy
[31] Los Alamos National Laboratory, Los Alamos, NM 87545, USA
[32] Santa Cruz Institute for Particle Physics, Department of Physics and Department of Astronomy and Astrophysics, University of California at Santa Cruz, Santa Cruz, CA 95064, USA; pablo@scipp.ucsc.edu
[33] Université de Bordeaux, Centre d'Études Nucléaires Bordeaux Gradignan, UMR 5797, Gradignan, 33175, France
[34] CNRS/IN2P3, Centre d'Études Nucléaires Bordeaux Gradignan, UMR 5797, Gradignan, 33175, France
[35] Arecibo Observatory, Arecibo, Puerto Rico 00612, USA
[36] Max-Planck-Institut für Radioastronomie, Auf dem Hügel 69, D-53121 Bonn, Germany

[37] Department of Physical Sciences, Hiroshima University, Higashi-Hiroshima, Hiroshima 739-8526, Japan
[38] Department of Physics and Department of Astronomy, University of Maryland, College Park, MD 20742, USA
[39] Istituto Nazionale di Fisica Nucleare, Sezione di Trieste, and Università di Trieste, I-34127 Trieste, Italy
[40] Center for Space Plasma and Aeronomic Research (CSPAR), University of Alabama in Huntsville, Huntsville, AL 35899, USA
[41] Department of Physics, Royal Institute of Technology (KTH), AlbaNova, SE-106 91 Stockholm, Sweden
[42] Australia Telescope National Facility, CSIRO, Epping NSW 1710, Australia
[43] Department of Physics, Tokyo Institute of Technology, Meguro City, Tokyo 152-8551, Japan
[44] Waseda University, 1-104 Totsukamachi, Shinjuku-ku, Tokyo, 169-8050, Japan
[45] Cosmic Radiation Laboratory, Institute of Physical and Chemical Research (RIKEN), Wako, Saitama 351-0198, Japan
[46] Centre d'Étude Spatiale des Rayonnements, CNRS/UPS, BP 44346, F-30128 Toulouse Cedex 4, France
[47] Istituto Nazionale di Fisica Nucleare, Sezione di Roma "Tor Vergata," I-00133 Roma, Italy
[48] Department of Physics and Astronomy, University of Denver, Denver, CO 80208, USA
[49] Max-Planck Institut für extraterrestrische Physik, 85748 Garching, Germany
[50] Institut für Astro- und Teilchenphysik and Institut für Theoretische Physik, Leopold-Franzens-Universität Innsbruck, A-6020 Innsbruck, Austria
[51] Eureka Scientific, Oakland, CA 94602, USA
[52] Institut de Ciencies de l'Espai (IEEC-CSIC), Campus UAB, 08193 Barcelona, Spain
[53] Space Sciences Division, NASA Ames Research Center, Moffett Field, CA 94035-1000, USA
[54] NYCB Real-Time Computing Inc., Lattingtown, NY 11560-1025, USA
[55] Department of Chemistry and Physics, Purdue University Calumet, Hammond, IN 46323-2094, USA
[56] Max-Planck-Institut für Kernphysik, D-69029 Heidelberg, Germany
[57] Institució Catalana de Recerca i Estudis Avançats (ICREA), Barcelona, Spain
[58] Consorzio Interuniversitario per la Fisica Spaziale (CIFS), I-10133 Torino, Italy
[59] Institute of Space and Astronautical Science, JAXA, 3-1-1 Yoshinodai, Sagamihara, Kanagawa 229-8510, Japan
[60] Unit for Space Physics, North-West University, Potchefstroom Campus, Potchefstroom 2520, South Africa
[61] Dipartimento di Fisica, Università di Roma "Tor Vergata," I-00133 Roma, Italy
[62] School of Pure and Applied Natural Sciences, University of Kalmar, SE-391 82 Kalmar, Sweden
Received 2009 October 9; accepted 2010 January 14; published 2010 February 5

ABSTRACT

We present multiwavelength studies of the 106.6 ms γ-ray pulsar PSR J1907+06 near the TeV source MGRO J1908+06. Timing observations with *Fermi* result in a precise position determination for the pulsar of R.A. = $19^{\rm h}07^{\rm m}54\overset{\rm s}{.}7(2)$, decl. = $+06^\circ02'16(2)''$ placing the pulsar firmly within the TeV source extent, suggesting the TeV source is the pulsar wind nebula of PSR J1907+0602. Pulsed γ-ray emission is clearly visible at energies from 100 MeV to above 10 GeV. The phase-averaged power-law index in the energy range $E > 0.1$ GeV is $\Gamma = 1.76 \pm 0.05$ with an exponential cutoff energy $E_c = 3.6 \pm 0.5$ GeV. We present the energy-dependent γ-ray pulsed light curve as well as limits on off-pulse emission associated with the TeV source. We also report the detection of very faint (flux density of $\simeq 3.4\,\mu$Jy) radio pulsations with the Arecibo telescope at 1.5 GHz having a dispersion measure DM = 82.1 ± 1.1 cm^{-3} pc. This indicates a distance of 3.2 ± 0.6 kpc and a pseudo-luminosity of $L_{1400} \simeq 0.035$ mJy kpc^2. A *Chandra* ACIS observation revealed an absorbed, possibly extended, compact ($\lesssim 4''$) X-ray source with significant nonthermal emission at R.A. = $19^{\rm h}07^{\rm m}54\overset{\rm s}{.}76$, decl. = $+06^\circ02'14\overset{''}{.}6$ with a flux of $2.3^{+0.6}_{-1.4} \times 10^{-14}$ erg cm^{-2} s^{-1}. From archival *ASCA* observations, we place upper limits on any arcminute scale 2–10 keV X-ray emission of $\sim 1 \times 10^{-13}$ erg cm^{-2} s^{-1}. The implied distance to the pulsar is compatible with that of the supernova remnant G40.5−0.5, located on the far side of the TeV nebula from PSR J1907+0602, and the S74 molecular cloud on the nearer side which we discuss as potential birth sites.

Key words: gamma rays: general – pulsars: general – pulsars: individual (PSR J1907+0602) – supernovae: individual (SNR G40.5–0.5)

Online-only material: color figures

1. INTRODUCTION

The TeV source MGRO J1908+06 was discovered by the Milagro Collaboration at a median energy of 20 TeV in their survey of the northern Galactic plane (Abdo et al. 2007) with a flux ~80% of the Crab at these energies. It was subsequently detected in the 300 GeV–20 TeV range by the H.E.S.S. (Aharonian et al. 2009) and VERITAS (Ward 2008) experiments. The H.E.S.S. observations show the source HESS J1908+063 to be clearly extended, spanning $\sim 0\overset{\circ}{.}3$ of a degree on the sky with hints of energy-dependent substructure. A decade earlier, Lamb & Macomb (1997) cataloged a bright source of GeV emission from the EGRET data, GeV J1907+0557, which is positionally consistent with MGRO J1908+06. It is near, but inconsistent with, the third EGRET catalog (Hartman et al. 1999) source 3EG J1903+0550 (Roberts et al. 2001). The Large Area Telescope (LAT; Atwood et al. 2009) aboard the *Fermi Gamma-Ray Space Telescope* has been operating in survey mode since soon after its launch on 2008 June 11, carrying out continuous observations of the GeV sky. The *Fermi* Bright Source List (Abdo et al. 2009b), based on 3 months of survey data, contains 0FGL J1907.5+0602 which is coincident with GeV J1907+0557. The 3EG J1903+0550 source location confidence contour stretches between 0FGL J1907.5+0602 and the nearby source 0FGL J1900.0+0356, suggesting it was a conflation of the two sources.

The *Fermi* LAT Collaboration recently reported the discovery of 16 previously unknown pulsars by using a time differencing technique on the LAT photon data above 300 MeV (Abdo et al. 2009a). 0FGL J1907.5+0602 was found to pulse with a period of 106.6 ms, have a spin-down energy of $\sim 2.8 \times 10^{36}$ erg s^{-1}, and was given a preliminary designation of PSR J1907+06. In this

---

[63] National Research Council Research Associate

[64] Royal Swedish Academy of Sciences Research Fellow, funded by a grant from the K. A. Wallenberg Foundation.

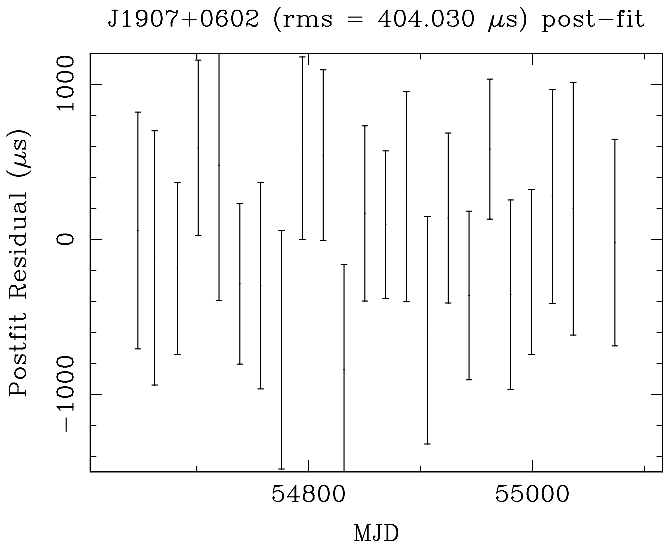

Figure 1. Post-fit timing residuals for PSR J1907+0602. The reduced χ^2 of the fit is 0.5.

Table 1
Measured and Derived Timing Parameters of PSR J1907+0602

Parameter	Value
Fit and data set	
Pulsar name	J1907+0602
MJD range	54647–55074
Number of TOAs	23
rms timing residual (μs)	404
Measured quantities	
Right ascension, α	19:07:54.71(14)
Declination, δ	+06:02:16.1(23)
Pulse frequency, ν (s^{-1})	9.3780713067(19)
First derivative of pulse frequency, $\dot{\nu}$ (s^{-2})	$-7.6382(4)\times10^{-12}$
Second derivative of pulse frequency, $\ddot{\nu}$ (s^{-3})	$2.5(6)\times10^{-22}$
Epoch of frequency determination (MJD)	54800
Dispersion measure (DM; cm^{-3} pc)	82.1(11)
Derived quantities	
Characteristic age (kyr)	19.5
Surface magnetic field strength (G)	3.1×10^{12}
$\dot{E}$ (erg s^{-1})	2.8×10^{36}
Assumptions	
Time units	TDB
Solar system ephemeris model	DE405

Notes. The numbers in parentheses are the errors in the last digit of the fitted parameters. The errors are statistical only, except for the position error, as described in Section 2. The derived parameters of $\dot{E}$, B, and τ_c are essentially unchanged with respect to those reported by Abdo et al. (2009a), but the position has moved by $1'.2$.

paper, we derive a coherent timing solution using 14 months of data which yields a more precise position for the source, allowing detailed follow-up at other wavelengths, including the detection of radio pulsations using the Arecibo 305 m radio telescope. Energy-resolved light curves, the pulsed spectrum, and off-pulse emission limits at the positions of the pulsar and pulsar wind nebula (PWN) centroid are presented. We then report the detection of an X-ray counterpart with the *Chandra X-ray Observatory* and an upper limit from *ASCA*. Finally, we discuss the pulsar's relationship to the TeV source and to the potential birth sites SNR G40.5−0.5 and the S74 H II region.

2. GAMMA-RAY PULSAR TIMING AND LOCALIZATION

The discovery and initial pulse timing of PSR J1907+06 were reported by Abdo et al. (2009a). The source position used in that analysis (R.A. = $286^\circ\!.965$, decl. = $6^\circ\!.022$) was derived from an analysis of the measured directions of LAT-detected photons in the on-pulse phase interval from observations made from 2008 August 4 to December 25. Here, we make use of a longer span of data and also apply improved analysis methods to derive an improved timing ephemeris for the pulsar as well as a more accurate source position.

For the timing and localization analysis, we selected "diffuse" class photons (events that passed the tightest background rejection criteria; Atwood et al. 2009) with zenith angle $< 105^\circ$ as is standard practice and chose the minimum energy and extraction radius to optimize the significance of pulsations. We accepted photons with $E > 200$ MeV from within a radius of $0^\circ\!.7$ of the nominal source direction. We corrected these photon arrival times to terrestrial time (TT) at the geocenter using the LAT Science Tool[65] `gtbary` in its geocenter mode.

We fitted a timing model using TEMPO2(Hobbs et al. 2006) to 23 pulse times of arrival (TOAs) covering the interval from 2008 June 30 to 2009 September 18. We note that during the on-orbit checkout period (before 2008 August 4) several instrument configurations were tested that affected the energy resolution and event reconstruction but had no effect on the LAT timing. To determine the TOAs, we generated pulse profiles by folding the photon times according to a provisional ephemeris using polynomial coefficients generated by TEMPO2 in its predictive mode (assuming a fictitious observatory at the geocenter). The TOAs were measured by cross-correlating each pulse profile with a kernel density template that was derived from fitting the full mission data set (P. S. Ray et al. 2010, in preparation). Finally, we fitted the TOAs to a timing model that included position, frequency, and frequency derivative. The resulting timing residuals are 0.4 ms and are shown in Figure 1. The best-fit model is displayed in Table 1. The numbers in parentheses are the errors in the last digit of the fitted parameters. The errors are statistical only, except for the position error, as described below. The derived parameters of $\dot{E}$, B, and τ_c are essentially unchanged with respect to those reported by Abdo et al. (2009a), but the position has moved by $1'.2$.

The statistical error on the position fit is $<1''$; however, this is an underestimate of the true error. For example, with only one year of data, timing noise can perturb the position fit. We have performed a Monte Carlo analysis of these effects by simulating fake residuals using the FAKE plugin for TEMPO2. We generated models with a range of frequency second derivatives ($\pm 2 \times 10^{-22}\ \mathrm{s}^{-3}$, the allowed magnitude for $\ddot{\nu}$ in our fits) to simulate the effects of timing noise and fitted them to timing models. Based on these simulations, we assigned an additional systematic error on the position of $2''$, which we added in quadrature to the statistical error in Table 1. As a result of the improved position estimate provided by this timing analysis, we have adopted a more precise name for the pulsar of PSR J1907+0602.

3. DETECTION OF RADIO PULSATIONS

To search for radio pulsations, we observed the timing position of PSR J1907+0602 with the L-wide receiver on the

---

[65] http://fermi.gsfc.nasa.gov/ssc/data/analysis/documentation/index.html

Arecibo 305 m radio telescope. On 2009 August 21, we made a 55 minute pointing with a center frequency of 1.51 GHz and a total bandwidth of 300 MHz, provided by three Wideband Arecibo Pulsar Processors (WAPPs; Dowd et al. 2000), each individually capable of processing 100 MHz. We divided this band into 512 channel spectra accumulated every 128 μs. The small positional uncertainty of PSR J1907+0602 derived from the LAT timing means that a single Arecibo pointing covers the whole region of interest (ROI).

After excising strong sources of radio-frequency interference with `rfifind`, one of the routines of the PRESTO signal analysis package (Ransom et al. 2002), we performed a search by folding the raw data with the *Fermi* timing model into 128 bin pulse profiles. We then used the PRESTO routine `prepfold` to search trial dispersion measures (DMs) between 0 and 1000 pc cm^{-3}. We found a pulsed signal with a signal-to-noise ratio, S/N = 9.4[66] and a duty cycle of about 0.03 at a dispersion measure, DM = 82.1 ± 1.1 cm^{-3} pc. This value was estimated by dividing the detection data into three sub-bands and making TOAs for each sub-band and fitting for the DM with TEMPO.

We applied the same technique for four different time segments of 12.5 minutes each and created a TOA for each of them. We then estimated the barycentric periodicity of the detected signal from these TOAs. This differs from the periodicity predicted by the LAT ephemeris for the time of the observation by (−0.000005 ± 0.000020) ms, i.e., the signals have the same periodicity.

Subsequent radio observations showed that the phase of the radio pulses is exactly as predicted by the LAT ephemeris, apart from a constant phase offset (depicted in Figure 2).

A confirmation observation with twice the integration time (1.8 hr) was made on 2009 September 4. The radio profile is shown in the bottom panel of Figure 2 with an arbitrary intensity scale. The pulsar is again detected with S/N of 3.4, 5.1, 7.3, and 8.6 at 1170, 1410, 1510, and 1610 MHz. The higher S/N at the higher frequencies suggest a positive spectral index, similar to what has been observed for PSR J1928+1746 (Cordes et al. 2006). However, this might instead be due to scattering degrading the S/N at the lowest frequencies—for the band centered at 1610 MHz the pulse profile is distinctively narrower (about 2% at 50% power) than at 1410 or 1510 MHz (about 3%). At 1170 MHz, the profile is barely detectable but very broad. This suggests an anomalously large scattering timescale for the DM of the pulsar. Observations at higher frequencies will settle the issue of the positive spectral index. For the 300 MHz centered at 1410 MHz, where the detection is clear, we obtain a total S/N of 12.4.

With an antenna $T_{\rm sys}$ = 33 K (given by the frequency-dependent antenna temperature of 25–27 K off the plane of the Galaxy plus 6 K of Galactic emission in the specific direction of the pulsar; Haslam et al. 1982), gain = 10.5 K Jy^{-1}, and two polarizations, and an inefficiency factor of 12% due to the three-level sampling of the WAPP correlators, we obtain for the first detection a flux density at 1.4 GHz of $S_{1400} \simeq 4.1\,\mu$Jy and for the second detection $S_{1400} \simeq 3.1\,\mu$Jy. These values are consistent given the large relative uncertainties in the S/N estimates and the varying effect of radio-frequency interference; at this DM, scintillation is not likely to cause a large variation in the flux density.

The time-averaged flux density is $\simeq 3.4\,\mu$Jy. Using the NE2001 model for the electron distribution in the Galaxy (Cordes & Lazio 2002), we obtain from the pulsar's position and DM a distance of 3.2 kpc with a nominal error of 20% (Cordes & Lazio 2002). The time-averaged flux density thus corresponds to a pseudo-luminosity $L_{1400} \simeq 0.035$ mJy kpc^2. This is fainter than the least luminous young pulsar in the ATNF catalog (PSR J0205+6449, with a 1.4 GHz pseudo-luminosity of 0.5 mJy kpc^2). It is, however, more luminous than the radio pulsations discovered through a deep search of another pulsar first discovered by *Fermi*, PSR J1741−2054 which has $L_{1400} \sim 0.025$ mJy kpc^2 (Camilo et al. 2009). These two detections clearly demonstrate that some pulsars, as seen from the Earth, can have extremely low apparent radio luminosities; i.e., similarly deep observations of other γ-ray selected pulsars might detect additional very faint radio pulsars. We note that these low luminosities, which may well be the result of only a faint section of the radio beam crossing the Earth, are much lower than what has often been termed "radio quiet" in population synthesis models used to estimate the ratio of "radio-loud" to "radio-quiet" γ-ray pulsars (e.g., Gonthier et al. 2004).

4. ENERGY-DEPENDENT GAMMA-RAY PULSE PROFILES

The pulse profile and spectral results reported in this paper use the survey data collected with the LAT from 2008 August 4 to 2009 September 18. We selected "diffuse" class photons (see Section 2) with energies $E > 100$ MeV and, to limit contamination from photons from Earth's limb, with zenith angle $< 105°$.

To explore the dependence of the pulse profile on energy, we selected an energy-dependent ROI with radius $\theta = 0.8 \times E^{-0.75}$ deg, but constrained not to be outside the range [0.°35, 1.°5]. We chose the upper bound to minimize the contribution from nearby sources and Galactic diffuse emission. The lower bound was selected in order to include more photons from the wings of the point-spread function (PSF) where the extraction region is small enough to make the diffuse contribution negligible. Figure 2 shows folded light curves of the pulsar in 32 constant-width bins for different energy bands. We use the centroid of the 1.4 GHz radio pulse profile to define phase 0.0. Two rotations are shown in each case. The top panel of the figure shows the folded light curve for photons with $E > 0.1$ GeV. The γ-ray light curve shows two peaks, P1 at phase 0.220 ± 0.002 which determines the offset with the radio peak, δ. The second peak in the γ-ray, P2, occurs at phase 0.580 ± 0.003. The phase separation between the two peaks is $\Delta = 0.360 \pm 0.004$. The radio lead δ and gamma peak separation Δ values are in good agreement with the correlation predicted for outer magnetosphere models, (Romani & Yadigaroglu 1995) and observed for other young pulsars (Figure 3 of A. A. Abdo et al. 2010, in preparation).

Pulsed emission from the pulsar is clearly visible for energies $E > 5$ GeV with a chance probability of $\sim 4 \times 10^{-8}$. Pulsed emission is detected for energies above 10 GeV with a confidence level of 99.8%. We have measured the integral and widths of the peaks as a function of energy and have found no evidence for significant evolution in shape or P1/P2 ratio with energy. We note that the pulsar is at low Galactic latitude ($b \sim -0.°89$)

---

[66] This was estimated using another software package, SIGPROC (a package developed by Duncan Lorimer; see http://sigproc.sourceforge.net/), which processes the bands separately and produced S/N of 4.2, 6.3, and 5.5 for the WAPPs centered at 1410, 1510, and 1610 MHz. Although S/N = 9.4 is close to the detection threshold for pulsars in a blind search, it is much more significant in this case because of the reduced number of trials in this search relative to a blind search.

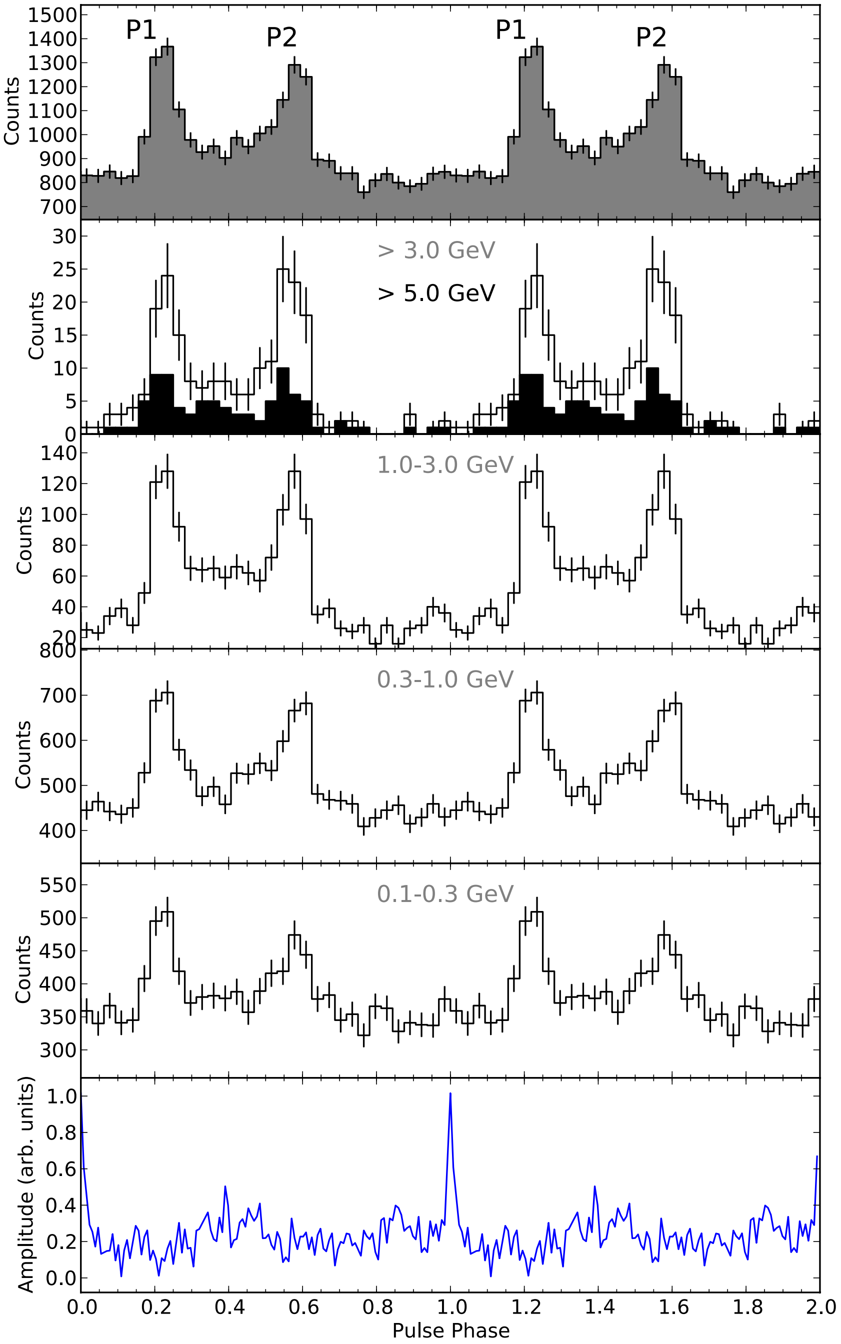

Figure 2. Folded light curves of PSR J1907+0602 in 32 constant-width bins for different energy bands and shown over two pulse periods with the 1.4 GHz radio pulse profile plotted in the bottom panel. The top panel of the figure shows the folded light curve for photons with $E > 0.1$ GeV. The other panels show the pulse profiles in exclusive energy ranges: $E > 3.0$ GeV (with $E > 5.0$ GeV in black) in the second panel from the top; 1.0–3.0 GeV in the next panel; 0.3–1.0 GeV in the fourth panel; and 0.1–0.3 GeV in the fifth panel.

where the Galactic γ-ray diffuse emission is bright (it has not been subtracted from the light curves shown.)

Figure 3 shows the observed LAT counts map of the region around PSR J1907+0602. We defined the "on" pulse as pulse phases $0.12 \leqslant \phi \leqslant 0.68$ and the "off" pulse as its complement ($0.0 \leqslant \phi < 0.12$ and $0.68 < \phi \leqslant 1.0$). We produced on-pulse (left panel) and off-pulse (right panel) images, scaling the off-pulse image by 1.27. The figure indicates the complexity of the region that must be treated in spectral fitting. Besides the pulsar, there are multiple point sources, Galactic, and extragalactic diffuse contributions.

5. ENERGY SPECTRUM

The phase-averaged flux of the pulsar was obtained by performing a maximum likelihood spectral analysis using the *Fermi* LAT science tool `gtlike`. Starting from the same data set described in Section 4, we selected photons from an ROI of 10° around the pulsar position. Sources from a preliminary version (based on 11 months of data) of the first *Fermi* LAT γ-ray catalog (A. A. Abdo et al. 2010, in preparation) that are within 15° ROI around the pulsar were modeled in this analysis. Spectra of sources farther away than 5° from the pulsar were fixed

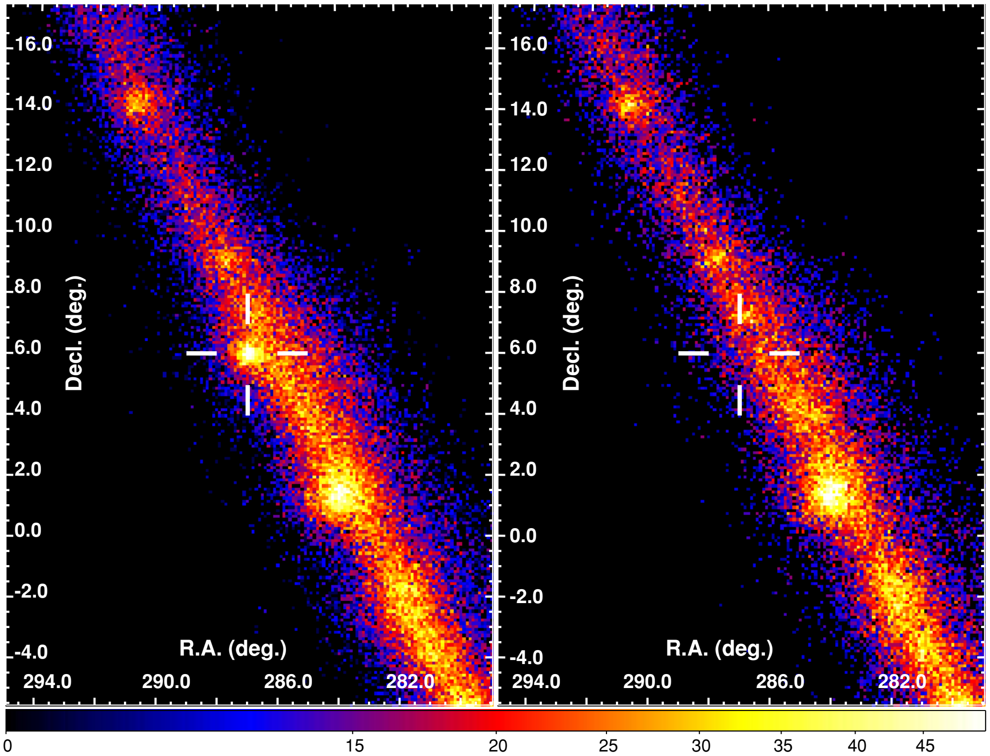

Figure 3. Observed *Fermi*-LAT counts map of the region around PSR J1907+0602. Left: "on"-pulse image, right: "off"-pulse image. The open cross-hair marks the location of the pulsar. Color scale shows the counts per pixel.

at the cataloged values. Sources within 5° of the pulsar were modeled with a simple power law. For each of the sources in the 5° region around the pulsar, we fixed the spectral index at the value in the catalog and fitted for the normalization. Two sources that are at a distance >5° showed strong emission and were treated in the same way as the sources within 5°. The Galactic diffuse emission (gll_iemv02) and the extragalactic diffuse background (isotropic_iem_v02) were modeled as well.[67]

The assumed spectral model for the pulsar is an exponentially cutoff power law: $dN/dE = N_o\,(E/E_o)^{-\Gamma}\exp(-E/E_c)$. The resulting spectrum gives the total emission for the pulsar assuming that the γ-ray emission is 100% pulsed. The unbinned `gtlike` fit, using P6_v3 instrument response functions (Atwood et al. 2009), for the energy range $E \geqslant 100$ MeV gives a phase-averaged spectrum of the following form:

$$\frac{dN}{dE} = \left(7.06 \pm 0.43_{\rm stat.} + \left(^{+0.004}_{-0.064}\right)_{\rm sys.}\right) \times 10^{-11} E^{-\Gamma} e^{-E/E_c} \times \gamma\ {\rm cm^{-2}\,s^{-1}\,MeV^{-1}}, \qquad (1)$$

where the photon index $\Gamma = 1.76 \pm 0.05_{\rm stat.} + (^{+0.271}_{-0.287})_{\rm sys.}$ and the cutoff energy $E_c = 3.6 \pm 0.5_{\rm stat.} + (^{+0.72}_{-0.36})_{\rm sys.}$ GeV.

The integrated energy flux from the pulsar in the energy range $E \geqslant 100$ MeV is $F_\gamma = (3.12 \pm 0.15_{\rm stat.} + (^{+0.16}_{-0.15})_{\rm sys.}) \times 10^{-10}$ erg cm^{-2} s^{-1}. This yields a γ-ray luminosity of $L_\gamma = 4\pi f_\Omega F_\gamma d^2 = 3.8 \times 10^{35} f_\Omega d_{3.2}^2$ erg s^{-1} above 100 MeV, where f_Ω is an effective beaming factor and $d_{3.2} = d/(3.2)$kpc. This corresponds to an efficiency of $\eta = L_\gamma/\dot{E} = 0.13 F_\gamma d_{3.2}^2$ for conversion of spin-down power into γ-ray emission in this energy band.

We set a 2σ flux upper limit on γ-ray emission from the pulsar in the off-pulse part of $F_{\rm off} < 8.31 \times 10^{-8}$ cm^{-2} s^{-1}. In addition to the γ-ray spectrum from the point-source pulsar PSR J1907+0602, we measured upper limits on γ-ray flux from the extended source HESS J1908+063 in the energy range 0.1–25 GeV. We performed binned likelihood analysis using the *Fermi* Science Tool `gtlike`. In this analysis, we assumed an extended source with a Gaussian width of $0^{\circ}\!.3$ and a γ-ray spectral index of −2.1 at the location of the H.E.S.S. source. The upper limits suggest that the spectrum of HESS J1908+063 has a low-energy turnover between 20 GeV and 300 GeV. Figure 4 shows the phase-averaged spectral energy distribution for PSR J1907+0602 (green circles). On the same figure, we show data points from H.E.S.S. for the TeV source HESS J1908+063 (blue circles) and the 2σ upper limits from *Fermi* for emission from this TeV source. Figure 5 shows an off-pulse residual map of the region around PSR J1907+0602. The timing position of the pulsar is marked by the green cross. The 5σ contours from Milagro (outer) and H.E.S.S. (inner) are overlaid. As can be seen from the residual map, there is no γ-ray excess at the location of either the pulsar or the PWN.

6. X-RAY COUNTERPART

A 23 ks *ASCA* Gas Imaging Spectrometer (GIS) exposure of the EGRET source GeV J1907+0557 revealed an ∼8′ × 15′ region of possible extended hard emission surrounding two point-like peaks lying ∼15′ to the southwest of PSR J1907+0602 (Roberts et al. 2001) and no other significant sources in the 44′ *ASCA* field of view (FOV). A 10 ks *Chandra* ACIS-I image of the *ASCA* emission (ObsID 7049) showed it to be dominated by a single hard point source, CXOU J190718.6+054858, with no compact nebular structure and just a hint of the several arcminute-scale emission seen by *ASCA*. CXOU J190718.6+054858 seemed to turn off for ∼2 ks during

---

[67] Descriptions of the models are available at http://fermi.gsfc.nasa.gov/.

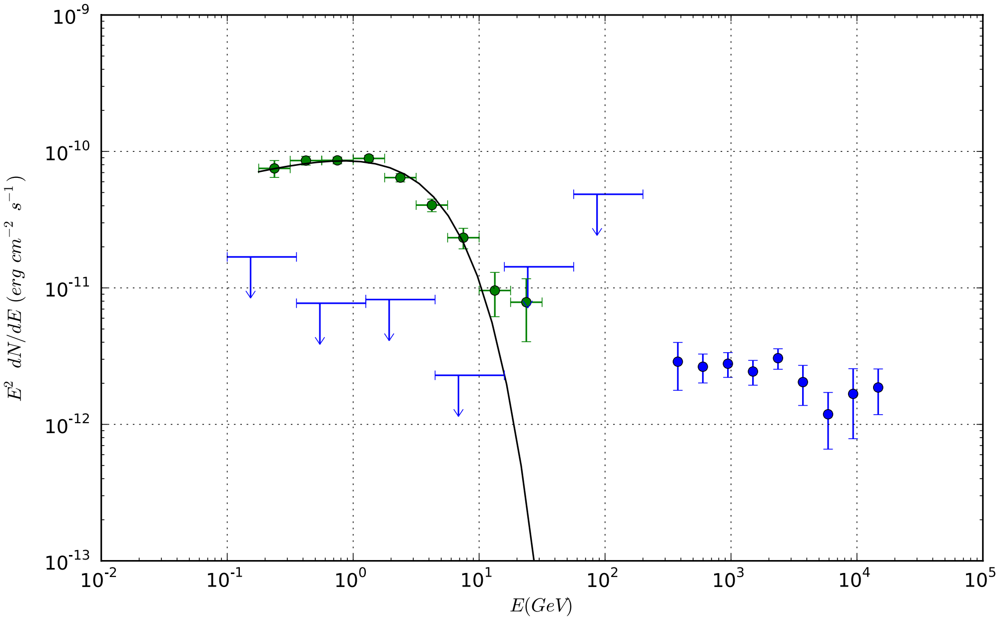

Figure 4. Phase-averaged spectral energy distribution for PSR J1907+0602 (green circles). Blue circles are data from H.E.S.S. for HESS J1908+063 TeV source. The 2σ upper limits from *Fermi* for emission from this TeV source are shown in blue. The black line shows the spectral model for the pulsar (Equation (1)). The upper limits suggest that the spectrum of HESS J1908+063 has a low-energy turnover between 20 GeV and 300 GeV.

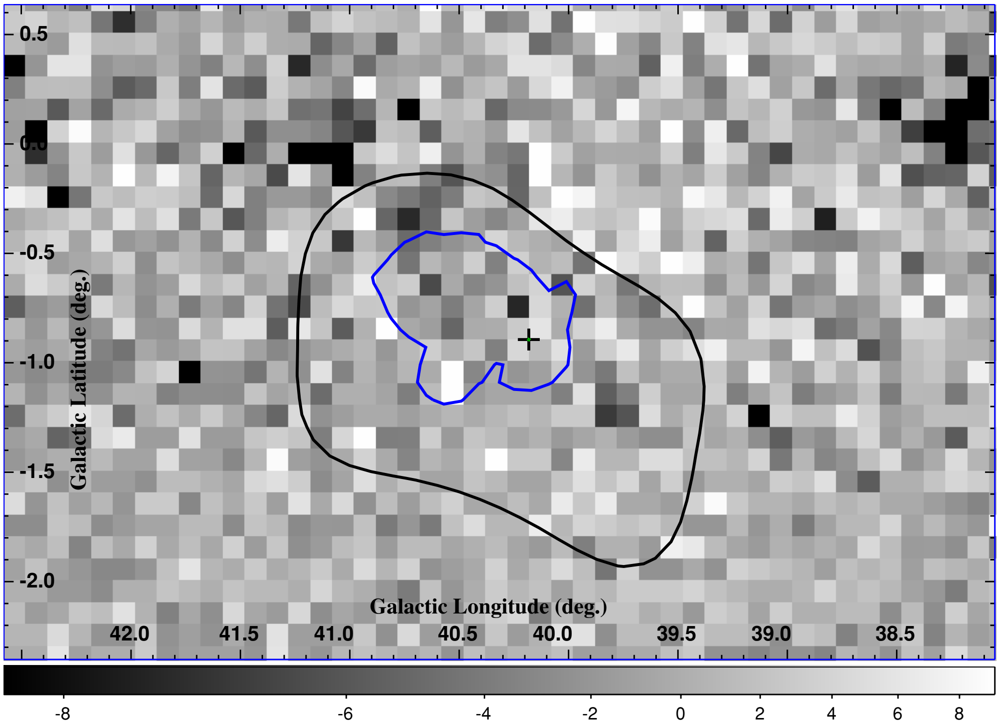

Figure 5. Residual map of the region around PSR J1907+0602 in the off pulse. The timing position of the pulsar is marked by the cross. The 5σ contours from Milagro (outer) and H.E.S.S. (inner) are overlaid.

the *Chandra* exposure, suggesting that it may be a binary of some sort or else a variable extragalactic source. There is no obvious optical counterpart in the digital sky survey optical or Two Micron All Sky Survey near infrared images, nor in an *I*-band image taken with the 2.4 m Hiltner Telescope at MDM (J. Halpern 2006, private communication). This strongly suggests that it is not a nearby source. An absorbed power-law fits the spectrum of this source well, with absorption $n_{\rm H} = 1.8^{+1.3}_{-0.9} \times 10^{22}$ cm^{-2} (90% confidence region), a photon spectral index $\Gamma = 0.9^{+0.6}_{-0.4}$, and an average 2–10 keV flux of $4.4^{+0.7}_{-1.8} \times 10^{-13}$ erg cm^{-2} s^{-1} (68% confidence region). The fit absorption is similar to the estimated total Galactic absorption from the HEASARC *n*H tool of 1.6×10^{22} cm^{-2} based on the Dickey & Lockman H I survey (Dickey & Lockman 1990), suggesting that an $n_{\rm H}$ of $\sim 2 \times 10^{22}$ cm^{-2} is a reasonably conservative estimate of interstellar absorption for sources deep in the plane along this line of sight.

The timing position of LAT PSR J1907+0602 is in the central 20′ of the *ASCA* GIS FOV (Figure 6). There is no obvious emission in the *ASCA* image at the pulsar position. Using

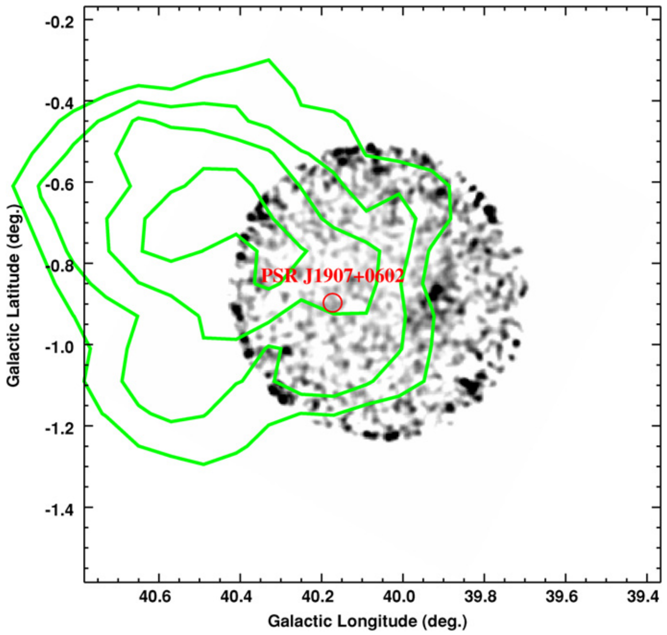

Figure 6. *ASCA* GIS 2-10 keV image of the region around PSR J1907+0602. The green contours are the 4σ–7σ significance contours from H.E.S.S.

(A color version of this figure is available in the online journal.)

the methodology of Roberts et al. (2001), a 24 pixel radius extraction region ($\sim 6'$), and assuming an absorbed power-law spectrum with $n_{\rm H} = 2 \times 10^{22}\,{\rm cm}^{-2}$ and $\Gamma = 1.5$, we place a 90% confidence upper limit on the 2–10 keV flux $F_x < 5 \times 10^{-14}\,{\rm erg\,cm^{-2}\,s^{-1}}$. This suggests that for any reasonable absorption, the total unabsorbed X-ray flux from the pulsar plus any arcminute-scale nebula is less than $10^{-13}\,{\rm erg\,cm^{-2}\,s^{-1}}$.

PSR J1907+0602 was well outside of the FOV of the first *Chandra* observation, and so we proposed for an observation centered on the pulsar. We obtained a 19 ks exposure with the ACIS-S detector (ObsID 11124). The time resolution of the ACIS-S detector on board *Chandra* does not allow for pulse studies. The only source within an arcminute of the timing position and the brightest source in the FOV of the S3 chip is shown in Figure 7. It is well within errors of the timing position. Examination of the X-ray image in different energy bands showed virtually no detected flux below ∼1 keV and significant flux above 2.5 keV, suggesting a nonthermal emission mechanism for much of the flux. A comparison of the spatial distribution of counts between 0.75 keV and 2 keV to those between 2 keV and 8 keV shows some evidence for spatial extent beyond the PSF for the harder emission but not for the softer emission. This would be consistent with an interpretation as predominantly absorbed but thermal emission from a neutron star surface surrounded by nonthermal emission from a compact PWN, which is the typical situation for young pulsars (see Kaspi et al. 2006, and references therein). We plot the *Chandra* 0.75–2 keV, 2–8 keV, and 0.75–8 keV images with an ellipse showing the timing position uncertainty, and a circle with a radius of $0''.8$. From a modeled PSF, we estimate that 80% of the counts should be contained within this circle. While this seems to be the case for the soft image, only roughly half the counts in the harder image are contained within that radius. With only ∼12 source counts in the 0.75–2 keV image within $6''$ and ∼30 source counts in the 2–8 keV image, quantitative statements about the source size and spectrum are difficult to make. We obtain a best-fit position for the nominal point source of R.A. = $19^{\rm h}07^{\rm m}54^{\rm s}.76$, decl. = $+06^\circ02'14''.6$, and an estimated error of $0''.7$ (an additional $0''.1$ centroid fitting uncertainty added to the nominal *Chandra* $0''.6$ uncertainty). Using a $6''$ radius extraction region and an annulus between $6''$ and $24''$ for the background, we extracted source and background spectra and fit them within XSPEC (Figure 8). A simple power law plus absorption model fit the data well in the energy range 2–10 KeV, with

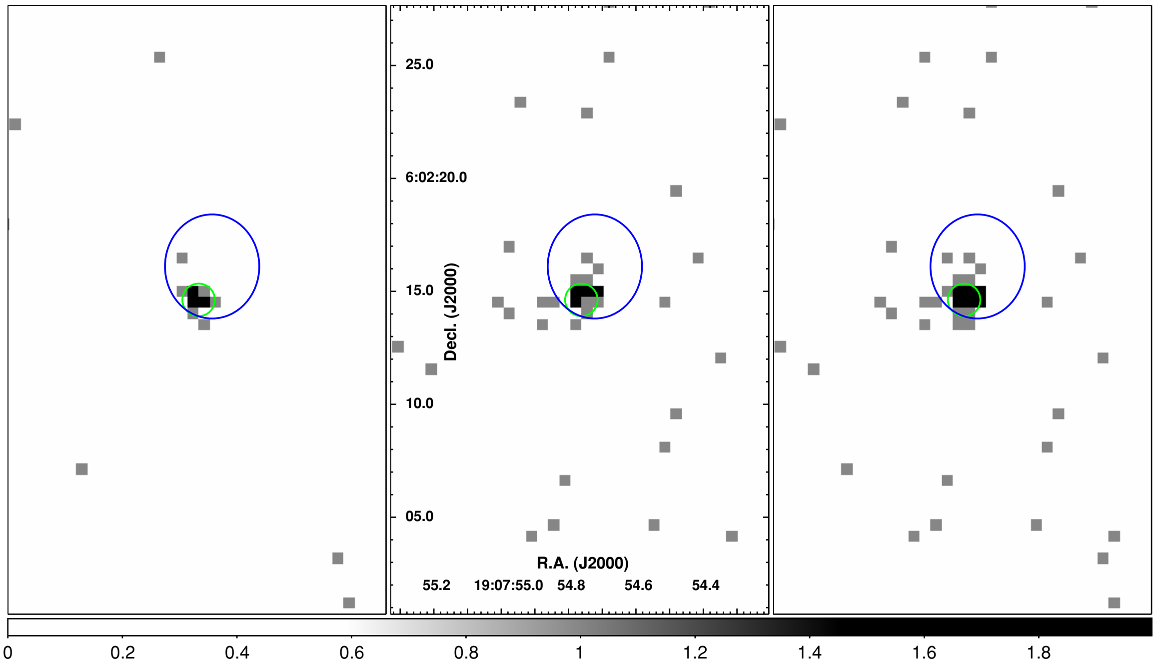

Figure 7. *Chandra* ACIS images of PSR J1907+0602. The blue ellipse shows the uncertainty in the timing position. The small green circle of radius $0''.8$ is twice the FWHM of the 5 keV PSF at this position, and should contain roughly 80% of the counts. The images at 0.75–2 keV (left), 2–8 keV (center), and 0.75–8 keV (right) are shown. Color scale shows the counts per pixel.

(A color version of this figure is available in the online journal.)

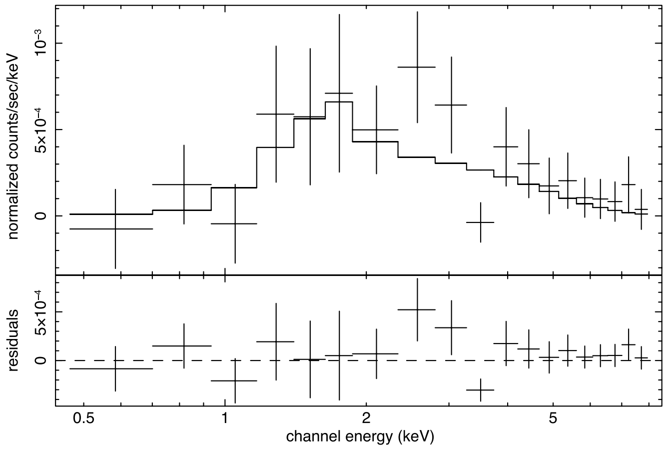

Figure 8. *Chandra* X-ray spectrum of PSR J1907+0602.

best-fit values $n_{\rm H} = 1.3 \times 10^{22}$ cm^{-2} and $\Gamma = 1.6$, with a total flux of $2.3^{+0.6}_{-1.4} \times 10^{-14}$ erg cm^{-2} s^{-1}. The low count rates and covariance between the absorption and photon index meant the spectral parameters could not be simultaneously meaningfully constrained. Fixing the spectral index $\Gamma = 1.6$, a typical value for compact PWNe (Kaspi et al. 2006), we obtain a 90% confidence region for the absorption of $(0.7\text{–}2.5) \times 10^{22}$ cm^{-2}, consistent with a source a few kiloparsecs or more away and with CXOU J190718.6+054858 discussed above. We note that with such an absorption a significant thermal component in the below 2 keV emission is neither required nor ruled out by the spectral fitting.

7. DISCUSSION

The DM from the radio detection suggests a distance of 3.2 kpc, with a nominal error of 20%. However, there are many outliers to the DM error distribution, although the largest fractional errors tend to be from pulsars at high Galactic latitudes or very low DMs (Deller et al. 2009; Chatterjee et al. 2009). For PSR J1907+0602, at a latitude $b = -0\overset{\circ}{.}9$ with a moderate DM, the distance estimate is likely to be reasonable. Since the apparent γ-ray pulsed efficiency in the *Fermi* passband is well above the median for other γ-ray pulsars in (Abdo et al. 2009c; 13% compared to 7.5%), it is worth checking secondary distance indicators to see if the DM could be a significant overestimate of the true distance. We can use the X-ray observations of PSR J1907+0602 to do this. Several authors have noted a correlation between the X-ray luminosity of young pulsars and their spin-down power (e.g., Saito 1997; Possenti et al. 2002; Li et al. 2008). Most of these have the problem of using X-ray fluxes derived from the literature using a variety of instruments with no uniform way of choosing spectral extraction regions. This can be especially problematic with *Chandra* data, since faint, arcminute-scale emission can easily be overlooked. We compare our *ASCA* GIS upper limits to Figure 1 of Cheng et al. (2004) who used only *ASCA* GIS data to derive their X-ray luminosity relationships. We see that the typical X-ray luminosity in the *ASCA* band for a pulsar with $\dot{E} = 2 \times 10^{36}$ erg s^{-1} is $L_x \sim 10^{33} - 10^{34}$ erg s^{-1} with all of the pulsars used in their analysis with $\dot{E} > 10^{36}$ erg s^{-1} having $L_x > 10^{32}$ erg s^{-1}. From these values and the *ASCA* upper limit, we derive a lower limit for the distance to LAT PSR J1907+0602 of $\sim$3 kpc. From Figure 2 of Li et al. (2008), who used *XMM-Newton* and *Chandra* derived values, we see we can expect the luminosity to be between $\sim 10^{31.5}$ and $10^{34.5}$ erg s^{-1}. From our detection with *Chandra*, we again estimate a lower distance limit of $\sim$3 kpc. The "best guess" estimate from their relationship would result in a distance of $\sim$13 kpc. We note that if we assume the pulsed emission to be apparently isotropic (i.e., $f_\Omega = 1$ as simple outer gap models suggest should approximately be the case; see Watters et al. 2009), a distance of 9 kpc would result in 100% γ-ray efficiency.

The derived timing position of PSR J1907+0602 is well inside the extended HESS source, although $\sim 14'$ southwest of the centroid. The TeV source is therefore plausibly the wind nebula of PSR J1907+0602. The physical size of this nebula is then $\gtrsim$40 pc, and the integrated luminosity above 1 TeV is $\gtrsim$40% that of the Crab, and in the Milagro band ($\sim$20 TeV) at least twice that of the Crab. There is a hint of some spatial dependence of the TeV spectrum in the H.E.S.S. data, with the harder emission (>2.5 TeV) peaking nearer the pulsar than the softer emission (Aharonian et al. 2009). If confirmed, this would be consistent with the hardening of the TeV emission observed toward PSR B1823−13, thought to be the pulsar powering HESS J1825−137 (Aharonian et al. 2006). This latter pulsar has a spin period, characteristic age, and spin-down energy similar to PSR J1907+0602, and is also located near the edge of its corresponding TeV nebula. We also note that HESS J1825−137 subtends $\sim 1^\circ$ on the sky and has a flux level above 1 TeV of around 20% of the Crab. While the overall spectrum of HESS J1825−137 is somewhat softer than the spectrum of HESS J1908+063, near the pulsar its spectrum is similarly hard. At a distance of $\sim$4 kpc, HESS J1825−137 has a luminosity similar to the Crab TeV nebula, but with a much larger physical size of $\sim$70 pc. Given the distance implied above and a flux above 1 TeV $\sim$ 17% of the Crab, HESS J1908+063 is similar in size and luminosity to HESS J1825−137.

At 20 TeV, HESS J1908+063 has a flux $\sim$80% of the Crab, and so at a distance $\gtrsim$1.5 times that of the Crab, and is much more luminous at the highest energies. This is because there is no sign of a high-energy cutoff or break, as is seen in many other TeV nebulae. Aharonian et al. (2009) place a lower limit of 19.1 TeV on any exponential cutoff to the spectrum. This implies that either the spectrum is uncooled due to a very low nebular magnetic field ($\lesssim 3\mu$G; see, e.g., de Jager 2008), an age much less than the characteristic age of 19.5 kyr, or else there is a synchrotron cooling break below the H.E.S.S. band.

Our upper limits above a few GeV (Figure 4) require there to be a low-energy turnover between 20 GeV and 300 GeV. Given the nominal PWN spectrum, we constrain the overall PWN flux to be $\leqslant$ 25% of that of the pulsar. If only the H.E.S.S. band is considered, and assuming the DM distance, the TeV luminosity $L_{\rm PWN} = 5\%\text{–}8\%\ \dot{E}$. However, since the TeV emission is generally thought to come from a relic population of electrons the luminosity is likely a function of the spin-down history of the pulsar rather than the current spin-down luminosity (e.g., de Jager 2008). These numbers support consistency of the association of the TeV source with the pulsar, in the weak sense of not being discrepant with other similar systems.

7.1. On the Possible Association with SNR G40.5−0.5

The bulk of HESS J1908+063 is between PSR J1907+0602 and the young radio SNR G40.5−0.5, suggesting a possible association. The distance estimate ($\sim$3.4 kpc; Yang et al. 2006) and age (Downes et al. 1980) estimates of SNR G40.5−0.5 are also consistent with those of PSR J1907+0602. If we use the usually assumed location for SNR G40.5−0.5 given by Langston et al. (2000; R.A. = $19^{\rm h}07^{\rm m}11\overset{\rm s}{.}9$, decl. = $6^\circ35'15''$),

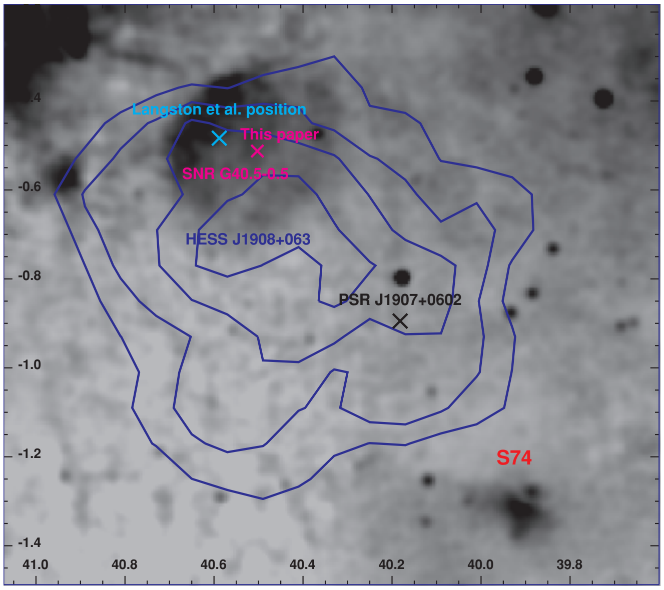

Figure 9. VGPS 1420 MHz image of region in Galactic coordinates showing relationship between SNR G40.5−0.5, HESS J1907+063 (blue contours representing the 4σ, 5σ, 6σ, and 7σ significance levels), the star-forming region S74, and PSR J1907+0602.

we get an angular separation of $\sim 35'$ between the timing position for the pulsar and the supernova remnant (SNR). However, this position for the SNR is from single dish observations that were offset toward one bright side of the nominal shell. We use the Very Large Array Galactic Plane Survey 1420 MHz image (Stil et al. 2006) of this region to estimate the SNR center to be R.A. $= 19^{\rm h}07^{\rm m}08\overset{\rm s}{.}6$, decl. $= 6°29'53''$ (Figure 9) which, for an assumed distance of 3.2 kpc, would give a separation of $\sim$28 pc. Given the characteristic age of 19.5 kyr, this would require an average transverse velocity of $\sim$1400 km s^{-1}. While velocities about this high are seen in some cases (e.g., PSR B1508+55 has a transverse velocity of $\sim$1100 km s^{-1}; Chatterjee et al. 2005), it is several times the average pulsar velocity and many times higher than the local sound speed. We note that pulsars with a braking index significantly less than $n = 3$ assumed in the derivation of the characteristic age could have ages as much as a factor of 2 greater (see, e.g., Kaspi et al. 2001), and thus a space velocity around half the above value may be all that is required. But with any reasonable assumption of birthplace, distance, and age, if the pulsar was born in SNR G40.5−0.5, any associated X-ray or radio PWN should show a bow shock and trail morphology, with the trail likely pointing back toward the SNR center. Unfortunately, the compactness and low number of counts in our *Chandra* image preclude any definite statement about the PWN morphology. One arrives at a different, and lower, minimum velocity if one assumes the pulsar was born at the center of the TeV PWN and moved to its present position, but the resulting velocity would still require a bow shock.

One can also get a pulsar offset toward the edge of a relic PWN if there is a significant density gradient in the surrounding interstellar medium (ISM). A gradient will cause the supernova blast wave to propagate asymmetrically. Where the density is higher, the reverse shock propagating back to the explosion center will also be asymmetric. This will tend to push the PWN away from the region of higher density (Blondin et al. 2001; Ferreira & de Jager 2008). This has been invoked to explain the offsets in the Vela X and HESS J1825−137 nebulae as well as several others. Infrared and radio imaging of the region shows that HESS J1908+063 borders on a shell of material surrounding the S74 H II region, also known as the Lynds Bright Nebula 352. Russeil (2003) gives a kinematic distance of 3.0 ± 0.3 kpc for this star-forming region, compatible with the pulsar distance. In this scenario, the pulsar would not have to be highly supersonic to be at the edge of a relic nebula, and would not have to be traveling away from the center of the TeV emission.

A third, hybrid possibility is that SNR G40.5−0.5 is only a bright segment of a much larger remnant, whose emission from the side near the pulsar is confused with that from the molecular cloud. The asymmetry would be explained by the difference in propagation speed in the lower density ISM away from the molecular cloud.

Our current *Chandra* data are insufficient to distinguish between the above scenarios. However, there is also the possibility of a compact cometary radio nebula, such as is seen around PSR B1853+01 in SNR W44 (Frail et al. 1996) and PSR B0906−49 (Gaensler et al. 1998). In addition, sensitive long wavelength radio imaging could reveal any larger, faint SNR shells. Imaging with the EVLA and Low Frequency Array of this region is therefore highly desirable. The connection between the pulsar and the TeV nebula could be further strengthened by a confirmation of the spatio-spectral dependence of the nebula where the spectrum hardens nearer to the pulsar.

The *Fermi* LAT Collaboration acknowledges the generous support of a number of agencies and institutes that have supported the *Fermi* LAT Collaboration. These include the National Aeronautics and Space Administration and the Department of Energy in the United States, the Commissariat à l'Energie Atomique and the Centre National de la Recherche Scientifique/Institut National de Physique Nucléaire et de Physique des Particules in France, the Agenzia Spaziale Italiana and the Istituto Nazionale di Fisica Nucleare in Italy, the Ministry of Education, Culture, Sports, Science and Technology (MEXT), High Energy Accelerator Research Organization (KEK) and Japan Aerospace Exploration Agency (JAXA) in Japan, and the K. A. Wallenberg Foundation and the Swedish National Space Board in Sweden. The Arecibo Observatory is part of the National Astronomy and Ionosphere Center, which is operated by Cornell University under a cooperative agreement with the National Science Foundation. The National Radio Astronomy Observatory is a facility of the National Science Foundation Operated under cooperative agreement by Associated Universities, Inc. Support for this work was provided by the National Aeronautics and Space Administration through *Chandra* Award Number GO6-7136X issued by the *Chandra* X-Ray Observatory Center, which is operated by the Smithsonian Astrophysical Observatory for and on behalf of NASA under contract NAS8-03060. This research has made use of software provided by the *Chandra* X-Ray Center in the application package CIAO. This research has made use of data obtained from the High Energy Astrophysics Science Archive Research Center (HEASARC), provided by NASA's Goddard Space Flight Center.

REFERENCES

Abdo, A. A., et al. (The Milagro Collaboration) 2007, ApJ, 664, L91
Abdo, A. A., et al. 2009a, Science, 325, 840 (Blind search pulsars)
Abdo, A. A., et al. 2009b, ApJS, 183, 46 (Bright source list)
Abdo, A. A., et al. 2009c, ApJ, submitted (Fermi catalog of gamma-ray pulsars)
Aharonian, F., et al. 2006, A&A, 460, 365
Aharonian, F., et al. 2009, A&A, 499, 723
Atwood, W. B., et al. 2009, ApJ, 697, 1071 (LAT)

Blondin, J. M., Chevalier, R. A., & Frierson, D. M. 2001, ApJ, 563, 806

Camilo, F., et al. 2009, ApJ, 705, 1 (Radio detection of two gamma-ray pulsars)

Chatterjee, S., et al. 2005, ApJ, 630, L61

Chatterjee, S., et al. 2009, ApJ, 698, 250

Cheng, K. S., Taam, R. E., & Wang, W. 2004, ApJ, 617, 480

Cordes, J. M., & Lazio, T. J. W. 2002, arXiv:astro-ph/0207156

Cordes, J. M., et al. 2006, ApJ, 637, 446

de Jager, O. C. 2008, ApJ, 678, L113

Deller, A. T., Tingay, S. J., Bailes, M., & Reynolds, J. E. 2009, ApJ, 701, 1243

Dickey, J. M., & Lockman, F. J. 1990, ARA&A, 28, 215

Dowd, A., Sisk, W., & Hagen, J. 2000, in ASP Conf. Ser. 202, IAU Coll. 177, Pulsar Astronomy-2000 and Beyond, ed. M. Kramer, N. Wex, & R. Wielebinski (San Francisco, CA: ASP), 275

Downes, A. J. B., Salter, C. J., & Pauls, T. 1980, A&A, 92, 47

Ferreira, S. E. S., & de Jager, O. C. 2008, A&A, 478, 17

Frail, D. A., Giacani, E. B., Goss, W. M., & Dubner, G. 1996, ApJ, 464, L165

Gaensler, B. M., Stappers, B. W., Frail, D. A., & Johnston, S. 1998, ApJ, 499, L69

Gonthier, P. L., Van Guilder, R., & Harding, A. K. 2004, ApJ, 604, 775

Hartman, R. C., et al. 1999, ApJS, 123, 79

Haslam, C. G. T., Salter, C. J., Stoffel, H., & Wilson, W. E. 1982, A&AS, 47, 1

Hobbs, G., Edwards, R., & Manchester, R. 2006, Chin. J. Astron. Astrophys. Suppl., 6, 189

Kaspi, V. M., Roberts, M. E., Vasisht, G., Gotthelf, E. V., Pivovaroff, M., & Kawai, N. 2001, ApJ, 560, 371

Kaspi, V. M., Roberts, M. S. E., & Harding, A. K. 2006, in Compact Stellar X-ray Sources, ed. W. H. G. Lewin & M. van der Klis (Cambridge: Cambridge Univ. Press), 279

Lamb, R. C., & Macomb, D. J. 1997, ApJ, 488, 872

Langston, G., Minter, A., D'Addario, L., Eberhardt, K., Koski, K., & Zuber, J. 2000, AJ, 119, 2801

Li, X.-H., Lu, F.-J., & Li, Z. 2008, ApJ, 682, 1166

Possenti, A., Cerutti, R., Colpi, M., & Mereghetti, S. 2002, A&A, 387, 993

Ransom, S. M., Eikenberry, S. S., & Middleditch, J. 2002, AJ, 124, 1788

Roberts, M. S. E., Romani, R. W., & Kawai, N. 2001, ApJS, 133, 451

Romani, R. W., & Yadigaroglu, I.-A. 1995, ApJ, 438, 314

Russeil, D. 2003, A&A, 397, 133

Saito, Y. 1997, PhD thesis, Univ. of Tokyo

Stil, J. M., et al. 2006, AJ, 132, 1158

Ward, J. E. 2008, in AIP Conf. Proc. 1085, High Energy Gamma-Ray Astronomy, ed. F. A. Aharonian, W. Hofmann, & F. Rieger (Melville, NY: AIP), 301

Watters, K. P., Romani, R. W., Weltevrede, P., & Johnston, S. 2009, ApJ, 695, 1289

Yang, J., Zhang, J.-L., Cai, Z.-Y., Lu, D.-R., & Tan, Y.-H. 2006, Chin. J. Astron. Astrophys., 6, 210